Water Supply

IWA PUBLISHING

Water Supply Vol 22 No 2, 1876 doi: 10.2166/ws.2021.308

Hydraulic characteristics of countercurrent jets on adverse-sloped beds

Lei Wang[a], Zhen Li[b] and Ming-jun Diao[a,*]

[a] State Key Laboratory of Hydraulics and Mountain River Engineering, Sichuan University, Chengdu 610065, China
[b] Department of Hydraulic Engineering, Sichuan Water Conservancy Vocational College, Dujiangyan 611800, China
*Corresponding author. E-mail: 2754239039@qq.com

ABSTRACT

The counter-current jet (CCJ) acts like a reverse surface jet layer covering the free jump surface and has potential applications in the energy dissipation of hydraulic engineering. The present study investigated the hydraulic characteristics of CCJs on adverse-sloped beds. The results showed that, compared to the horizontal bed, the slope didn't increase the energy dissipation rate of CCJ but reduced the return flow length and upstream depth. The velocity distribution along the depth was divided into the boundary layer region, mixing region, and reverse surface jet region. The velocity distribution in the boundary layer region and the mixing region was similar to the classical wall jet. The jet Froude number and the bed slope had no significant effect on the turbulence intensity distribution and turbulence kinetic energy (TKE) distribution of CCJ. The distribution of TKE was similar to that of a submerged jump. The maximum absolute turbulence intensity appeared at exactly half of the maximum velocity. The maximum TKE appeared at the mixing region. Besides, empirical formulas for estimating length scales and maximum velocity attenuation are proposed. The results could provide a reference for the potential application of CCJ in energy dissipation in hydraulic engineering.

Key words: adverse slope, countercurrent jet, energy dissipation, open channel, turbulence characteristics, velocity distribution

HIGHLIGHTS

- The hydraulic characteristics of counter-current jets (CCJ) on adverse-sloped beds were investigated for the first time.
- The velocity distribution of CCJ was divided into three regions along the depth.
- The turbulence intensity and turbulence kinetic energy distribution of CCJ had self-similarity.
- A new counter-current energy dissipator with potential applications was provided.

GRAPHICAL ABSTRACT

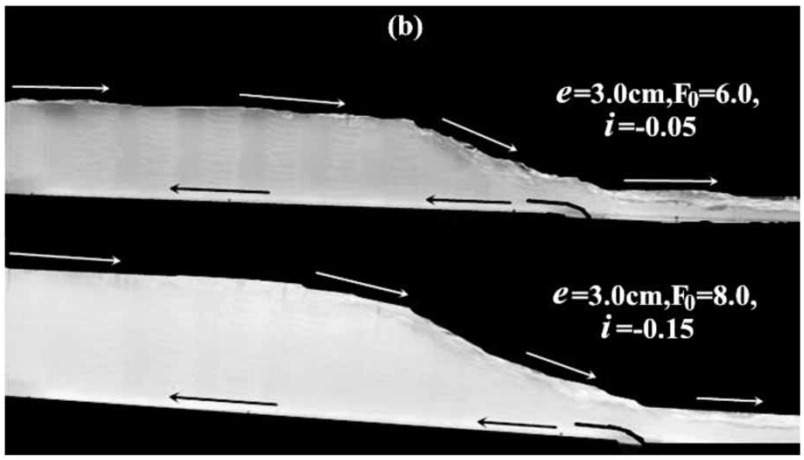

INTRODUCTION

The counter-current jet (CCJ) has significant practical application value in many fields. CCJ could be applied to heat transfer regulation (Volchkov *et al.* 1995), mixed chemicals and sewage (Ramamurthy *et al.* 2019), and drag reduction technology (Josyula *et al.* 2015). CCJ could also be used for energy dissipation in hydraulic engineering. Hager (1994) designed an open-flow countercurrent energy dissipator (CCED) using CCJ and investigated the hydraulic characteristics of CCJ on the horizontal bed. The result showed that the CCED could stabilize water flow, reduce the downstream channel scour and stilling basin length, and increase the energy dissipation rate, compared to the traditional stilling basin without auxiliary energy dissipators. Experimental observations showed that CCJ acted like a reverse surface jet layer covering the free jump surface. Wang & Diao (2021) further investigated the velocity distribution characteristics of CCJs on horizontal beds based on the research of Hager (1994). The maximum velocity decay was more efficient, and the velocity distribution was more even than in the classical jump. So far, these two papers are the only ones that have studied CCED. Although CCED had many advantages, the CCED type needed further research. Since CCJ was analogous to the classical jump, and the jumps on adverse-sloped beds reduced the sequent depth ratio and roller length compared to jumps on horizontal beds (McCorquodale & Mohamed 1994; Pagliara & Peruginelli 2000; Bateni & Yazdandoost 2009; Beirami & Chamani 2010), it was also worth studying the hydraulic characteristics of CCJ on the adverse-sloped bed. The research methods of the hydraulic jump were mainly experimental and numerical simulation or a combination of both (Wu & Rajaratnam 1995; Ead & Rajaratnam 2002a, 2002b; Lin *et al.* 2012; Dios *et al.* 2016; Witt *et al.* 2018; Ghaderi *et al.* 2020). The methodology and content of these studies of jumps had implications for the CCJ research.

Due to the potential practical value of CCED in energy dissipation of hydraulic engineering, a new type of CCED was designed using the CCJ on the adverse-sloped bed, drawing on previous research on hydraulic jumps on an adverse-sloped bed. Therefore, this paper carries out an exploratory experimental study of the hydraulic characteristics of CCJs on a reverse slope bed, taking into account the effects of bed slopes and jet Froude numbers. The differences in the length scale characteristics of CCJs on adverse-sloped and horizontal beds were compared. This paper also preliminarily investigated the self-similarity in the turbulence characteristics of CCJs. The results increased the understanding of CCJ and could provide some reference for the practical design.

METHODS

All the experiments were performed in a 5.0 m × 0.5 m × 1.0 m acrylic flume (Figure 1(a)). A pump with a maximum discharge of 200 L/s was used to feed the flume. A magnetic flow-meter with an accuracy of ±0.5% FS was installed on the circular pressure pipeline to adjust the discharges. A pressure water tank of 1.0 m × 0.5 m × 0.6 m connected the circular pipeline to the rectangular pipeline I. The rectangular pipeline II connected to the bend was 1.0 m long. A five-layer grid was installed in the rectangular pipeline II at 0.2 m intervals to smooth out the water flow. And the mesh opening size was 0.5 cm × 0.5 cm. Water entered the flume through a 90-degree bend whose radius was 10 cm. The bend was connected to a 10.0 cm long horizontal segment to ensure the streamlines were well oriented to the adverse slope bed, thereby producing a uniform jet with a thickness of e. The bend was iron prefabricated and replaceable, whose wall thickness was 1 mm. The adverse slope bed of 2.5 m × 0.499 m × 0.01 m was parallel to the horizontal segment and the water-tightness of the gate was guaranteed by glass cement. The tailwater freely flows outward without controlling the downstream depth h_d. A total of eight series tests ($S1$–$S8$) were carried out and the main parameters are shown in Table 1. The bed slope i ranged from −0.025 to −0.20. The jet Froude number $F_0 = u_0/(ge)^{0.5}$ was in the range of 4.0–10.0, and the Reynolds number $R_e = u_0 e/\nu$ was in the range of 35,440–162,750, where u_0 was the mean velocity of the slot, g was the acceleration of gravity, and ν was the kinematic viscosity of the fluid. Figure 1(b) showed the photos of tests $i = -0.05$, $F_0 = 6.0$, $e = 3.0$ cm ($S2$) and $i = -0.15$, $F_0 = 8.0$, $e = 3.0$ cm ($S6$), respectively.

For trunk tests $S2$ and $F_0 = 8.0$ ($S1$, $S2$ – $S7$), the ADV (Nortek Vectrino II) with an accuracy of ±0.001 m/s measured velocity pulsations at any point to analyse the turbulence characteristics in CCJ on adverse-sloped beds, while for other tests, a propeller velocimeter with an accuracy of ±0.01 m/s was used to measure velocity profiles. To accurately calculate the turbulence parameters, the sampling frequency was 100 Hz and the sampling time was 5 minutes. The cylindrical control volume of the ADV was 6 mm in diameter and 2–15 mm in height, located 5 cm below the transmitter probe. A gradual lifting device with an accuracy of 1 mm controlled the ADV probe to determine the velocity measuring point, which could move parallel to the bed through a sliding rail. The propeller velocimeter was to measure the velocity within 5 cm below the

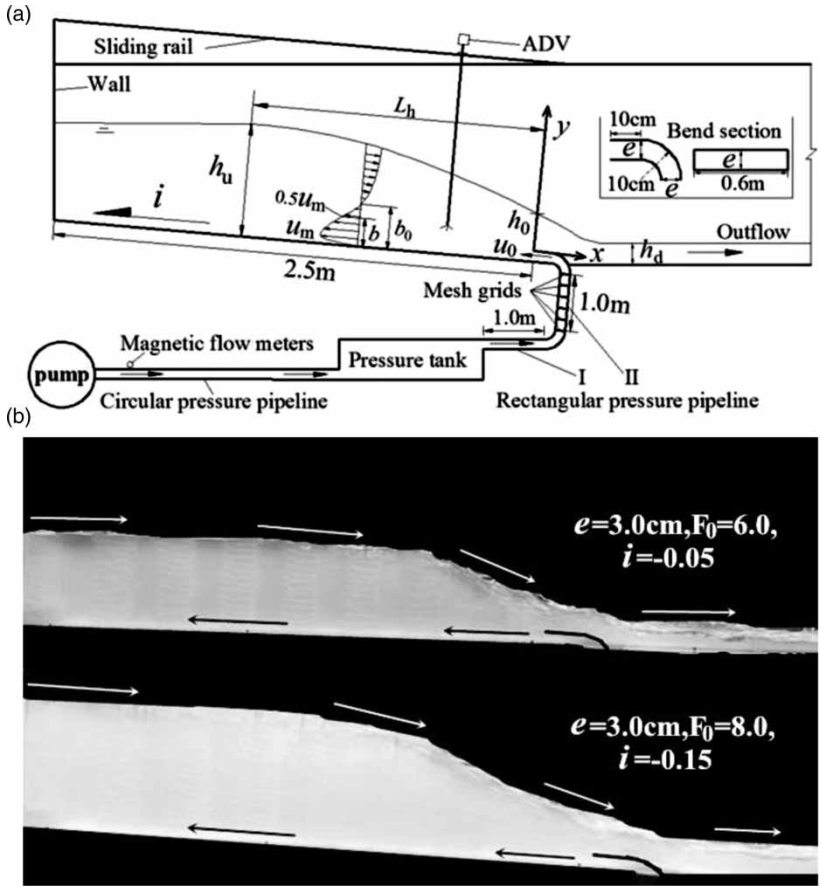

Figure 1 | (a) Schematic diagram; (b) Photos of the countercurrent jet.

water surface. Velocity time series data with SNR (signal-to-noise ratio) less than 15 dB were removed based on the instrument instructions. The iteration-free method proposed by Islam & Zhu (2013) was to eliminate the burrs in the data series. Frizell (2000) and Liu *et al.* (2002) experimentally verified the measured flow velocity increased by about 5% over the unaerated flow velocity for low air concentrations. The bubble quantity in the countercurrent jet was negligible and the bubble volume was small. The effect of air bubbles on the velocity measurement was therefore negligible. Water surface profiles for all the tests were measured with a resistance wave gauge (CBG01) to an accuracy of 0.1 mm. Water surface profiles were sampled for 5 minutes at a sampling frequency of 100 Hz. The ADV probe and wave gauge shared the gradual lifting device installed in the central plane of the flume. After a certain distance from the slot, the water surface was almost horizontal. This distance was defined as the return flow length L_h, and the water depth at $x = -L_h$ was upstream depth h_u. The water depth on the bend at $x = 0$ was h_0. Since the bend wall thickness was only 1 mm, its effect on the water depth was negligible. All tests measured water surface profiles and velocity profiles. The vertical interval of the velocity measurement point was 1.0 cm. The velocity distribution was measured in 9–11 sections for every trunk test. Table 2 showed the velocity sections of the trunk tests. Dey *et al.* (2010) verified that the flow was reasonably two-dimensional in the center plane of the flume and the flow near the side walls was essentially three-dimensional. All velocity measurement points were in the center plane of the flume, so the flow in the center plane of the flume could be regarded as two-dimensional.

RESULTS AND DISCUSSION

Geometrical properties

Similar to the classical jump, for a CCJ on the adverse-sloped bed, the upstream and downstream water depth ratio h_u/h_d may be affected by the jet thickness e, the mean velocity u_0 of the slot, and the bed slope i. Therefore, the ratio h_u/h_d can be

Table 1 | Main parameters of tests

Tests	F_0	i	u_0(m/s)	e(cm)	Re	h_u	h_0	h_d(cm)	L_h(cm)
S1	4.0	− 0.025	2.170	3.0	65,100	22.5	7.0	4.9	54.0
	5.0	− 0.025	2.712	3.0	81,360	26.0	7.4	5.4	72.9
	6.0	− 0.025	3.255	3.0	97,650	31.0	8.0	6.0	90.5
	7.0	− 0.025	3.798	3.0	1,13,940	35.0	8.6	6.5	105.6
	8.0	− 0.025	4.338	3.0	1,30,140	39.5	9.0	7.0	123.0
	9.0	− 0.025	4.880	3.0	1,46,400	43.8	9.5	7.5	138.0
	10.0	− 0.025	5.425	3.0	1,62,750	48.0	10.0	7.9	154.2
S2	5.0	− 0.05	2.712	3.0	81,360	24.4	7.6	5.3	64.0
	6.0	− 0.05	3.255	3.0	97,650	28.7	8.5	6.0	79.2
	7.0	− 0.05	3.798	3.0	1,13,940	32.8	9.1	6.5	94.9
	8.0	− 0.05	4.338	3.0	1,30,140	36.9	9.6	7.0	110.0
	9.0	− 0.05	4.880	3.0	1,46,400	40.6	10.1	7.5	124.2
	10.0	− 0.05	5.425	3.0	1,62,750	44.8	10.6	7.9	142.7
S3	5.0	− 0.075	2.712	3.0	81,360	22.5	7.7	5.3	61.8
	6.0	− 0.075	3.255	3.0	97,650	27.0	9.0	6.0	80.7
	7.0	− 0.075	3.798	3.0	1,13,940	30.0	9.7	6.5	94.5
	8.0	− 0.075	4.338	3.0	1,30,140	34.2	10.1	7.0	105.3
	9.0	− 0.075	4.880	3.0	1,46,400	37.8	10.2	7.5	120.3
	10.0	− 0.075	5.425	3.0	1,62,750	42.0	10.8	7.9	135.0
S4	5.0	− 0.1	2.712	3.0	81,360	21.1	8.4	5.3	60.6
	6.0	− 0.1	3.255	3.0	97,650	25.0	9.0	6.0	74.1
	7.0	− 0.1	3.798	3.0	1,13,940	28.4	9.7	6.5	89.0
	8.0	− 0.1	4.338	3.0	1,30,140	32.2	10.3	7.0	102.5
	9.0	− 0.1	4.880	3.0	1,46,400	35.7	10.9	7.5	117.0
	10.0	− 0.1	5.425	3.0	1,62,750	39.6	11.4	7.9	129.6
S5	5.0	− 0.125	2.712	3.0	81,360	20.0	8.0	5.3	59.4
	6.0	− 0.125	3.255	3.0	97,650	23.2	8.7	6.0	71.5
	7.0	− 0.125	3.798	3.0	1,13,940	26.6	9.7	6.5	82.2
	8.0	− 0.125	4.338	3.0	1,30,140	30.0	10.4	7.0	97.8
	9.0	− 0.125	4.880	3.0	1,46,400	33.9	11.1	7.5	111.5
	10.0	− 0.125	5.425	3.0	1,62,750	37.2	11.3	7.9	122.0
S6	5.0	− 0.15	2.712	3.0	81,360	19.5	8.3	5.3	55.8
	6.0	− 0.15	3.255	3.0	97,650	23.4	8.9	6.0	65.9
	7.0	− 0.15	3.798	3.0	1,13,940	26.3	9.5	6.5	78.1
	8.0	− 0.15	4.338	3.0	1,30,140	29.2	10.1	7.0	92.2
	9.0	− 0.15	4.880	3.0	1,46,400	32.5	10.6	7.5	107.4
	10.0	− 0.15	5.425	3.0	1,62,750	35.6	11.0	7.9	120.6
S7	5.0	− 0.2	2.712	3.0	81,360	18.6	8.0	5.3	52.0
	6.0	− 0.2	3.255	3.0	97,650	21.1	8.9	5.9	65.6
	7.0	− 0.2	3.798	3.0	1,13,940	23.7	9.6	6.5	77.5
	8.0	− 0.2	4.338	3.0	1,30,140	26.7	10.2	7.0	90.5
	9.0	− 0.2	4.880	3.0	1,46,400	29.2	10.7	7.5	101.3
	10.0	− 0.2	5.425	3.0	1,62,750	32.0	11.2	7.9	114.5
S8	4.0	− 0.025	1.772	2.0	35,440	15.0	4.8	3.3	36.6
	5.0	− 0.05	2.215	2.0	44,300	16.0	5.4	3.6	42.2
	6.0	− 0.075	2.658	2.0	53,160	17.6	6.3	3.9	53.0
	7.0	− 0.1	3.100	2.0	62,000	19.2	6.7	4.4	58.4
	8.0	− 0.125	3.543	2.0	70,860	20.6	7.2	4.7	65.6
	9.0	− 0.15	3.986	2.0	79,720	21.2	7.3	5.0	71.0
	10.0	− 0.2	4.430	2.0	88,600	21.5	7.6	5.3	76.3

Table 2 | Velocity sections of trunk tests

Test	$F_0 = 5.0$	$F_0 = 6.0$	$F_0 = 7.0$	$F_0 = 8.0$	$F_0 = 9.0$	$F_0 = 10.0$
$e = 3.0$ cm $i = -0.05$	$x = -0.1$ m	$x = -0.1$ m	$x = -0.1$ m	$x = -0.1$ m	$x = -0.1$ m	$x = -0.1$ m
	$x = -0.2$ m	$x = -0.2$ m	$x = -0.2$ m	$x = -0.2$ m	$x = -0.2$ m	$x = -0.2$ m
	$x = -0.3$ m	$x = -0.3$ m	$x = -0.3$ m	$x = -0.3$ m	$x = -0.35$ m	$x = -0.3$ m
	$x = -0.4$ m	$x = -0.4$ m	$x = -0.45$ m	$x = -0.5$ m	$x = -0.5$ m	$x = -0.4$ m
	$x = -0.5$ m	$x = -0.5$ m	$x = -0.6$ m	$x = -0.7$ m	$x = -0.65$ m	$x = -0.55$ m
	$x = -0.6$ m	$x = -0.65$ m	$x = -0.75$ m	$x = -0.9$ m	$x = -0.8$ m	$x = -0.7$ m
	$x = -0.7$ m	$x = -0.8$ m	$x = -0.9$ m	$x = -1.1$ m	$x = -1.0$ m	$x = -0.85$ m
	$x = -0.8$ m	$x = -0.95$ m	$x = -1.05$ m	$x = -1.3$ m	$x = -1.2$ m	$x = -1.05$ m
	$x = -0.9$ m	$x = -1.1$ m	$x = -1.2$ m	$x = -1.5$ m	$x = -1.4$ m	$x = -1.25$ m
	$x = -1.0$ m	$x = -1.25$ m	$x = -1.35$ m		$x = -1.6$ m	$x = -1.45$ m
	$x = -1.1$ m	$x = -1.4$ m	$x = -1.5$ m			$x = -1.6$ m
Test	$i = -0.025$	$i = -0.075$	$i = -0.10$	$i = -0.125$	$i = -0.15$	$i = -0.20$
$e = 3.0$ cm $F_0 = 8.0$	$x = -0.1$ m	$x = -0.1$ m	$x = -0.1$ m	$x = -0.1$ m	$x = -0.1$ m	$x = -0.1$ m
	$x = -0.2$ m	$x = -0.2$ m	$x = -0.2$ m	$x = -0.2$ m	$x = -0.2$ m	$x = -0.2$ m
	$x = -0.3$ m	$x = -0.3$ m	$x = -0.3$ m	$x = -0.3$ m	$x = -0.3$ m	$x = -0.3$ m
	$x = -0.45$ m	$x = -0.4$ m	$x = -0.4$ m	$x = -0.4$ m	$x = -0.4$ m	$x = -0.4$ m
	$x = -0.6$ m	$x = -0.55$ m	$x = -0.6$ m	$x = -0.5$ m	$x = -0.5$ m	$x = -0.5$ m
	$x = -0.75$ m	$x = -0.7$ m	$x = -0.8$ m	$x = -0.6$ m	$x = -0.65$ m	$x = -0.6$ m
	$x = -0.9$ m	$x = -0.85$ m	$x = -1.0$ m	$x = -0.75$ m	$x = -0.8$ m	$x = -0.7$ m
	$x = -1.05$ m	$x = -1.0$ m	$x = -1.2$ m	$x = -0.9$ m	$x = -0.95$ m	$x = -0.85$ m
	$x = -1.2$ m	$x = -1.2$ m	$x = -1.4$ m	$x = -1.05$ m	$x = -1.1$ m	$x = -1.0$ m
	$x = -1.35$ m	$x = -1.4$ m		$x = -1.2$ m	$x = -1.3$ m	$x = -1.2$ m
	$x = -1.5$ m	$x = -1.6$ m		$x = -1.35$ m		

expressed as:

$$h_u/h_d = f_1(e, u_0, g, \rho, \nu, i) \tag{1}$$

where ρ was water density. Using the Pi theorem, the ratio h_u/h_d can be written as:

$$h_u/h_d = f_2(F_0 = u_0/\sqrt{ge}, R_e = u_0 e/\nu, i) \tag{2}$$

In this study, the Reynolds number R_e was in the range of 35,440–162,750, which was relatively high. The viscous effects were negligible at high Reynolds numbers (Hager & Bremen 1989). Thus, Equation (2) can be reduced to the following form:

$$h_u/h_d = f_3(F_0, i) \tag{3}$$

Similarly, the ratio h_u/e can be written as:

$$h_u/e = f_4(F_0, i) \tag{4}$$

The return flow length L_h was also can be expressed as:

$$L_h/e = f_5(F_0, i) \tag{5}$$

Upstream depth h_u observations are shown in Figure 2(a)–2(d). As shown in Figure 2(a) and 2(c), for $i = -0.025$, the values of ratios h_u/e and h_u/h_d were not much different from those of CCJs on horizontal beds (Wang & Diao 2021). The downstream channel was horizontal for the present study, which hindered the development of CCJ. The results also showed that the values of ratios h_u/e and h_u/h_d were 7.5%–34.5% and 6.0%–32.0% less than those of CCJs on horizontal beds for $i < -0.05$ (Wang & Diao 2021), respectively. The ratios h_u/e and h_u/h_d increased with the jet Froude number F_0 and

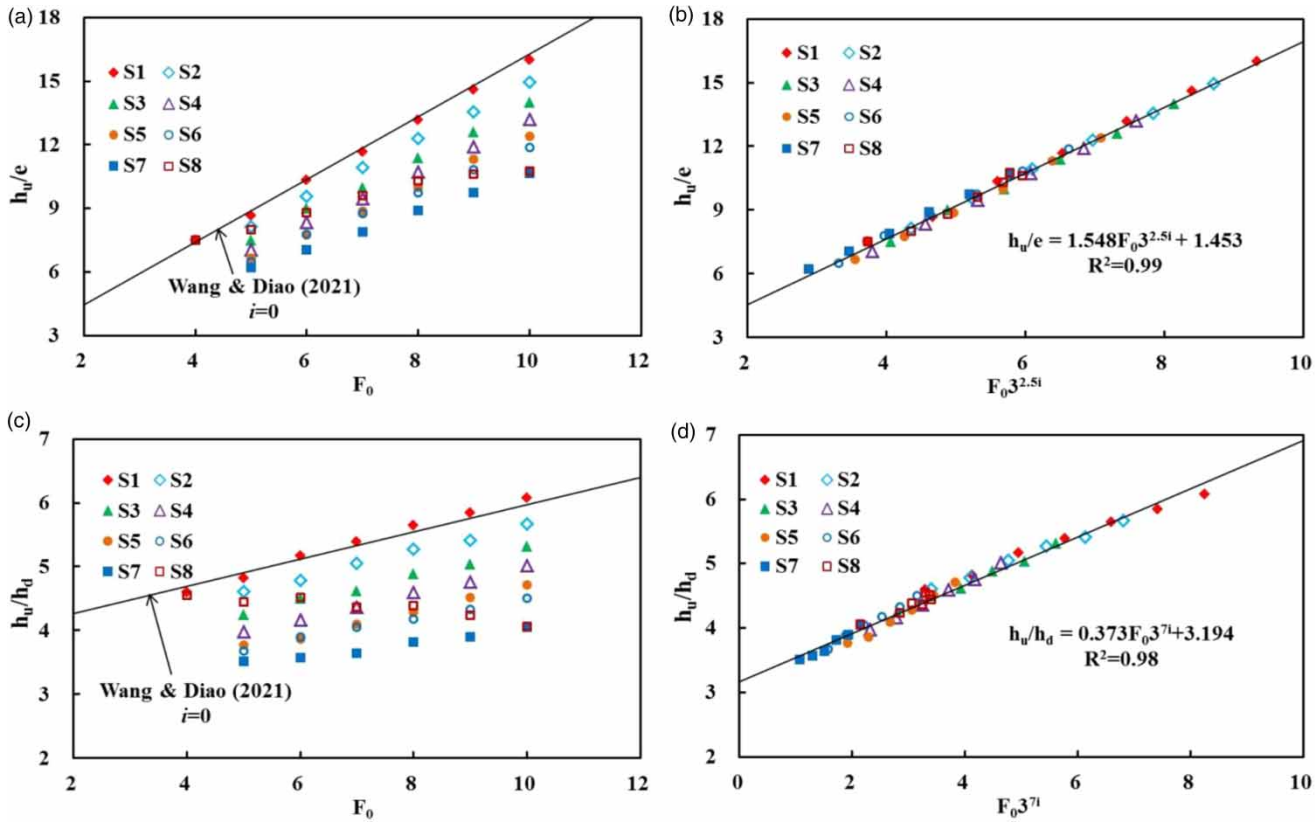

Figure 2 | Variation of (a) h_u/e against F_0; (b) h_u/e against $F_03^{2.5i}$; (c) h_u/h_d against F_0; (d) h_u/h_d against F_03^{7i}.

decreased with the bed slope i. The experimental observations of the ratios h_u/e and h_u/h_d were replotted against the parameters $F_03^{2.5i}$ and F_03^{7i} in Figure 2(b) and 2(d), respectively. These relationships are described by the following equations, respectively:

$$h_u/e = 1.548F_03^{2.5i} + 1.453, \ -0.2 \le i < 0 \tag{6}$$

$$h_u/h_d = 0.373F_03^{7i} + 3.194, \ -0.2 \le i < 0 \tag{7}$$

From Figure 3(a), the variation trend of the return flow length L_h was similar to the upstream depth h_u. The ratio L_h/e was 11.0%–28.5% less than that for CCJ on the horizontal bed for $i < -0.05$ (Wang & Diao 2021). The ratio L_h/e was plotted

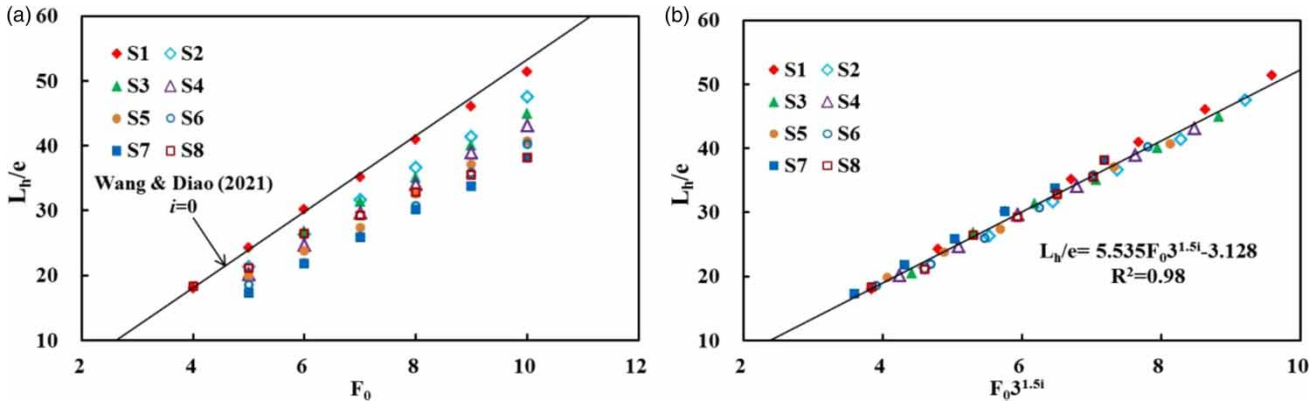

Figure 3 | Variation of L_h/e against (a) F_0; (b) $F_03^{1.5i}$.

against the parameter $F_0 3^{1.5i}$ in Figure 3(b) and the following equation:

$$L_h/e = 5.535F_0 3^{1.5i} - 3.128, \ -0.2 \le i < 0 \tag{8}$$

The present results showed that the adverse-sloped bed could reduce the upstream depth h_u and return flow length L_h of CCJ compared to the horizontal bed. It could reduce the size of the engineering design and reduce the cost of the engineering.

Velocity distribution

Figure 4(a) and 4(b) showed typical mean velocity distributions of CCJs on adverse-sloped beds for the trunk tests were analogous to those of the classical jump (Wu & Rajaratnam 1995). The parameter b and the maximum velocity of section u_m were chosen as the length and velocity scales, respectively, to test the velocity distribution similarity of the classical jump. The parameter b was the distance between the point $u = 0.5u_m$ ($\partial u/\partial y < 0$) and the bed (Wu & Rajaratnam 1995), where u was the mean velocity at any point. For test series $S2$, the variations of u/u_m against y/b were plotted in Figure 4(c). For $F_0 = 8.0$, Figure 4(d) showed the effect of the bed slope on the velocity distribution similarity. The observations from

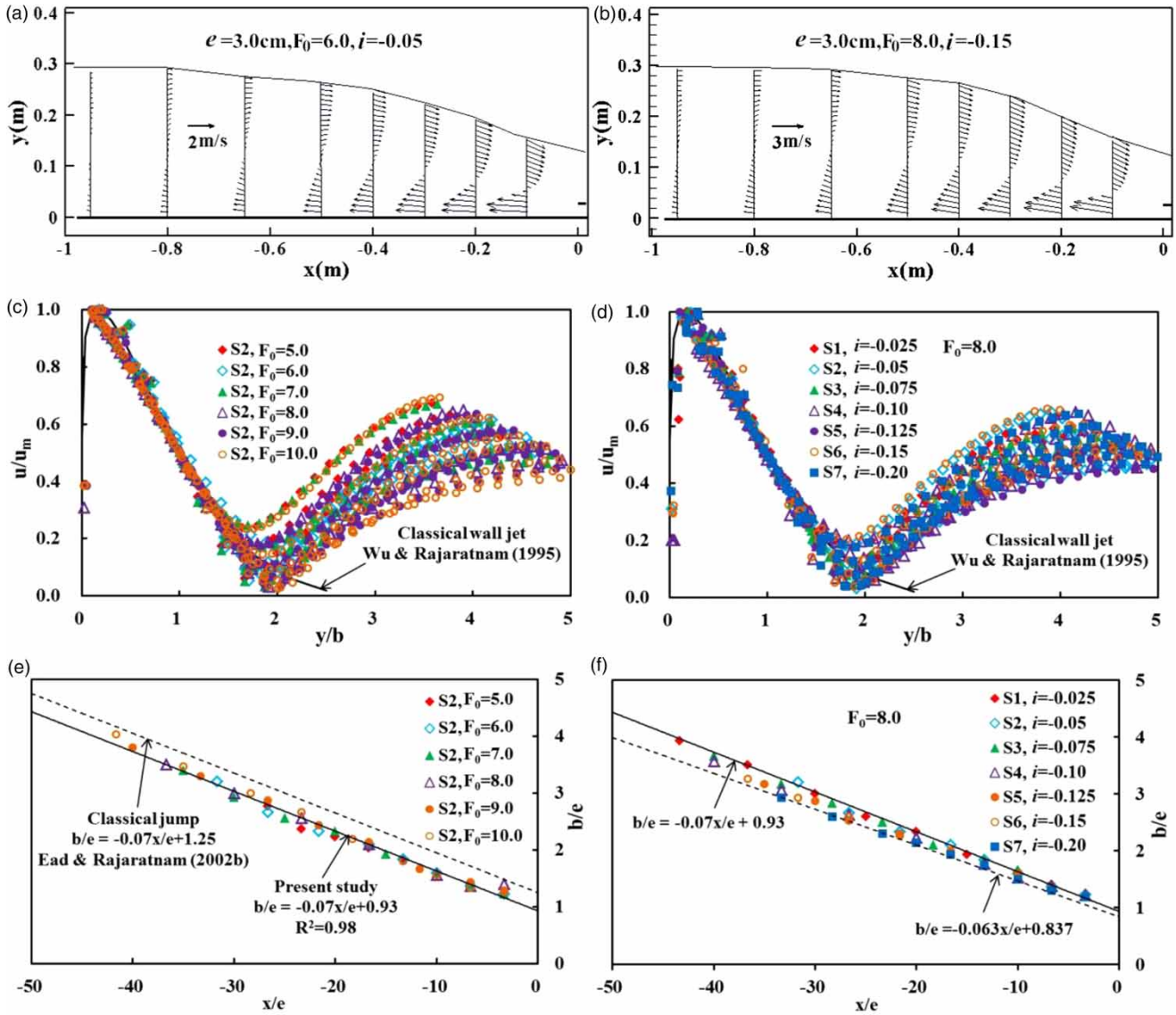

Figure 4 | (a-b) Typical mean velocity distributions of CCJ; (c-d) Similarity profile of mean velocity ($-0.1\ \text{m} < x < L_h$); (c-d) y/b against u/u_m; (e-f) Variation of b/e against x/e.

Figure 4(c) and 4(d) showed that the velocity distribution was analogous to the curve of classical wall jet for $y/b < 2.0$ (Wu & Rajaratnam 1995) and was not significantly affected by the jet Froude number and bed slope. However, the velocity distribution was significantly different from the classical wall jet for $y/b > 2.0$. The present results showed that the velocity increased with the parameter y/b in the boundary layer. The velocity decreased first and then increased with the depth outside the boundary layer. Thus the velocity distribution along with the depth could be divided into three regions: the boundary layer region where $0 < y \leq \delta$ (δ was the boundary layer thickness); the mixing region where $\delta < y < 2.0b$; reverse surface jet region $y > 2.0b$. The velocity increased with the boundary layer thickness in the boundary layer region, decreased with the depth in the mixing region, and increased in the reverse surface jet region. Figure 4(e) showed that for $i = -0.05$, the growth rate of b/e with x/e was approximately equal to 0.07 at different jet Froude numbers. This growth rate was slightly less than 0.076 for a submerged jump on the smooth bed and was equal to the value of 0.07 for classical jumps (Ead & Rajaratnam 2002a, 2002b). The observations presented that the value of b/e for $i = -0.05$ was 7.0%–25.0% less than that of the classical jump. Figure 4(f) showed that for $F_0 = 8.0$, the growth rate of b/e with x/e decreased as the bed slope increased, and this growth rate was in the range of -0.07 to -0.063. Figure 4(f) also showed that the growth rate was approximately the same for $i = -0.025$ and $i = -0.05$. Figure 4(e) and 4(f) showed that the growth of b with x was mainly affected by a bed slope lower than -0.05. The value of b/e for $i = -0.2$ was 10.0% less than that for $i = -0.05$.

As shown in Figure 5(a) and 5(b), the jet Froude number and bed slope had no significant effect on the maximum velocity decay. The decay process could be represented by one mean curve which was expressed by the following equation:

$$u_m/u_0 = 0.12(x/L)^2 + 0.74x/L + 1.11 \tag{9}$$

The length scale L was the value of x at which $u_m = 0.5u_0$. The decay curve of CCJ was slightly less than that of the free jump on the horizontal bed (Wu & Rajaratnam 1995) for $-1.5 < x/L < 0$. And for $x/L < -1.5$, the difference between the two was getting larger. Figure 5(c) showed that the variation trend of length scale L was similar to the return flow length L_h. The ratio of L/e was 3.0%–20.5% less than that for CCJ on the horizontal bed for $i < -0.05$ (Wang & Diao 2021).

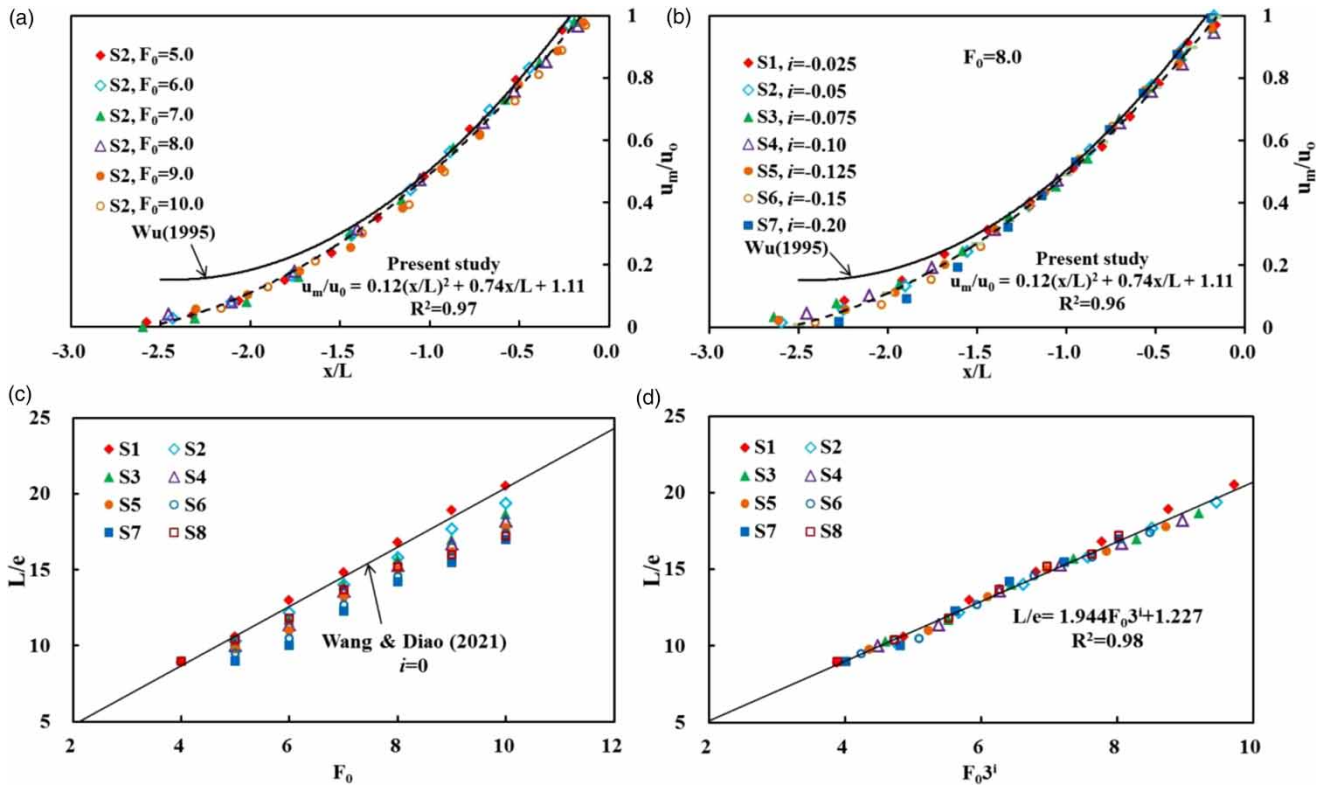

Figure 5 | Variation of (a-b) u_m/u_0 against x/L; variation of L/e against (c) F_0; (d) $F_0 3^{3i}$.

The results showed that the adverse-sloped bed was very effective in reducing the longitudinal length scale and increasing the velocity decay rate of CCJ. The ratio L/e was plotted against the parameter $F_0 3^i$ in Figure 5(d) and the following equation

$$L/e = 1.994F_0 3^i + 1.227, \ -0.2 \le i \le 0 \tag{10}$$

Bed shear stress and energy loss

It was verified that the bed shear stress was the main cause of energy loss for the hydraulic jump (Ead & Rajaratnam 2002b; Bejestan & Neisi 2009). Therefore, it is necessary to study the bed shear stress of CCJ on the adverse-sloped bed. Take the control volume as shown in Figure 6(a), and the integral momentum equation considering the integrated bed shear stress F_τ can be written as:

$$F_\tau = 0.5\varepsilon\rho g e^2 = 0.5\rho g(e^2 + h_0^2 - h_u^2) + \rho q(u_0 + q/h_0) + W\sin\theta \tag{11}$$

The shear force coefficient ε of CCJ can be written as:

$$\varepsilon = \frac{e^2 + h_0^2 - h_u^2}{e^2} + \frac{q(u_0 + q/h_0)}{0.5ge^2} + \frac{kL_h(e + h_0 + h_u)}{e^2}\sin\theta \tag{12}$$

In Equation (11) and Equation (12), q = unit discharge; θ = the angle of the bed slope ($i = -\tan\theta$); W = weight of the water in the control volume for unit width, $W = k\rho g L_h(e + h_0 + h_u)/2$; $k = S_{ABCDE}/S_{ABDE}$ = coefficient for determination of weight. According to Equation (12), the variation of shear force coefficients ε against F_0 is shown in Figure 6(b). The coefficient ε increased with F_0 and decreased as i increased. The increase of bed shear stress led to the decrease of upstream depth h_u. Therefore, the ratios of h_u/e and h_u/h_d decreased with the bed slope i. Compared to the CCJ on the horizontal bed (Wang & Diao 2021), the value of ε for the present study was larger when the bed slope i was less than -0.05. As F_0 increased,

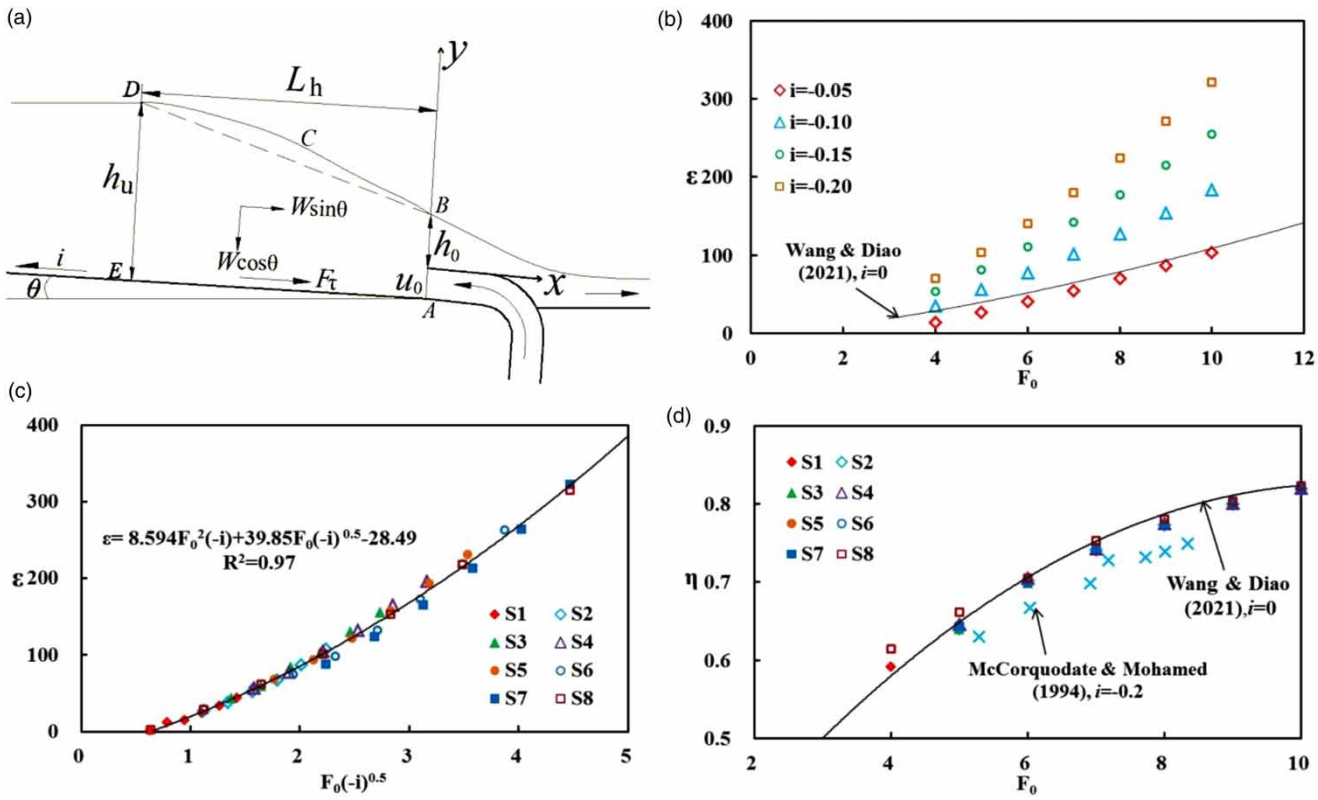

Figure 6 | (a) Schematic diagram of control volume; (b, c) Variation of ε against $F_0(-i)^{0.5}$; (d) Variation of η against F_0.

the difference between the coefficient ε on the horizontal bed and that on the adverse-sloped bed increased. The observations of coefficients ε were replotted against the parameters $F_0(-i)^{0.5}$ in Figure 6(c) and the following equation:

$$\varepsilon = 8.594F_0^2(-i) + 39.85F_0(-i)^{0.5} - 28.49 \quad (13)$$

The energy dissipation ratio η of CCJ was defined as $\eta = (E_2 - E_1)/E_1$, where $E_1 = e + h_0 + u_0^2/2g$ and $E_2 = h_d + q^2/(2gh_d^2)$. As shown in 6(c), the energy dissipation ratio of CCJ on the adverse-sloped bed was not significantly different from that on the horizontal bed (Wang & Diao 2021), which meant that the adverse-sloped bed had a limited effect on increasing the energy dissipation rate of CCJ. Compared with CCJ on the horizontal bed, although the bed shear stress on the adverse-sloped bed increased, the adverse-slope increased the potential energy of CCJ. Therefore, the energy dissipation rate of CCJ on the flat and adverse-sloped bed was not much different. It is worth mentioning that the adverse-sloped bed also could not increase the energy dissipation rate of the free jump in contrast to the horizontal bed (Bateni & Yazdandoost 2009; Beirami & Chamani 2010). It indicated that CCJ and the hydraulic jump shared some similarities in hydraulic characteristics. The results also showed that the energy dissipation ratio of CCJ on the adverse-sloped bed was 4.0%–7.0% larger than that of the free jump for $i = -0.2$ (McCorquodale & Mohamed 1994). Known from the velocity distribution of CCJ, the velocity direction in the mixing region was opposite to that in the reverse surface jet region. Therefore, the internal friction at the junction of the mixing region and reverse surface jet region was relatively large, led to an increase in the energy dissipation rate of CCJ compared to the free jump on the adverse-sloped bed.

Turbulence characteristics

The equivalent velocity pulsation intensity was defined as the absolute turbulence intensity (ATI) $\sigma = \sqrt{\overline{u_x'^2} + \overline{u_y'^2}}$, where u_x' and u_y'were the longitudinal and vertical velocity pulsations, respectively. Similar to the velocity distribution, the maximum ATI σ_m of the section and the parameter b were chosen as the intensity scale and length scale, respectively. From Figure 7(a) and 7(b), the jet Froude number and bed slope also had no significant effect on the similarity of ATI distribution. The variation of y/b against σ/σ_m could be represented by one mean curve. The observations also showed that the maximum ATI along water depth appeared at $y = b$, which happened to be $u = 0.5u_m$ ($\partial u/\partial y < 0$). ATI increased with the depth for $0 < y < b$ and decreased for $y > b$. Having found that the ATI distributions of CCJ are similar, it is necessary to study the similarity of the relative turbulence intensity (RTI) distributions. RTI was defined as $\sigma_r = \sigma/u$. As shown in Figure 7(c) and 7(d), like ATI, the jet Froude number and bed slope also had no significant effect on the RTI distribution. The RTI distributions of CCJ were similar except around the maximum RTI. The maximum RTI appeared at $y = 2.0b$, which happened to be the boundary between the mixing region and reverse surface jet region. RTI increased along with the depth for $0 < y < 2.0b$ and decreased for $y > 2.0b$. The flow direction of the reverse surface jet was opposite to that of the mainstream below, thereby resulting in a velocity gradient mutation at the junction of the mixing region and reverse surface jet region. Therefore the maximum RTI appeared at $y = 2.0b$ and then decayed up and down along the depth.

The turbulence kinetic energy (TKE) K at any point was defined as $K = 0.5(\overline{u_x'^2} + \overline{u_y'^2})$ (Dios *et al.* 2016). The maximum TKE K_m and the length scale b_K, defined as the value of y where $K = 0.5K_m$, were chosen to test for the similarity of TKE distributions of CCJ on the adverse-sloped bed. Figure 8(a) and 8(b) showed the variations of K/Km against y/b_K. The observations showed that the TKE distributions were similar and could be represented by the TKE distribution curve of the submerged jump (Dios *et al.* 2016). The formula proposed by Dios *et al.* (2016) that described this curve was:

$$K/K_m = 2.9(y/b_K)^{1/1.4}[1 - erf(1.17y/b_K)] + 0.23 \quad (14)$$

Figure 8(a) and 8(b) also showed that the jet Froude number and bed slope had little effect on the similarity of TKE distributions.

Having studied the similarity of TKE distributions, let us study the decay of maximum TKE. Figure 8(c) showed the variations of Km$^{0.5}/u_0$ against x/h_u and Km$^{0.5}/u_m$ against x/L_h, respectively. The decay rate of Km$^{0.5}/u_0$ with x/h_u was not affected by the jet Froude number and bed slope. The decay rate was approximately equal to 0.068, which was much larger than the value of 0.016 for a classical jump (Liu *et al.* 2004). The variations of Km$^{0.5}/u_m$ against x/L_h were similar. This relationship could be represented by the following regression equation:

$$K_m^{0.5}/u_m = 0.2485\exp(-x/L_h) \quad (15)$$

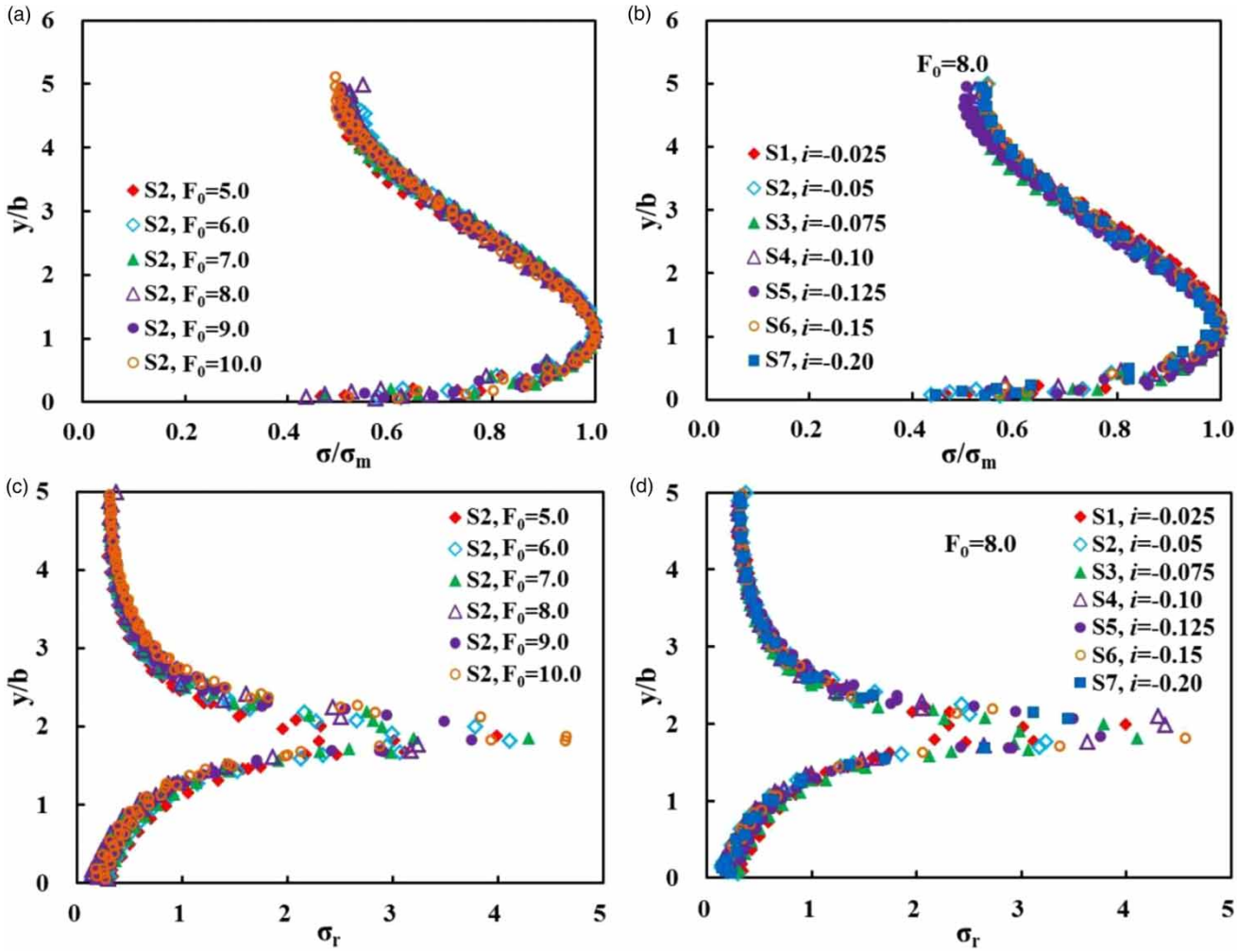

Figure 7 | Variation of y/b against (a-b) σ/σ_m; (c-d) σ_r.

Figure 8(d) showed the variation of various vertical length scale ratios with distance x/L_h, where δ_K was the value of y at $K = K_m$, and b_0 was the value of y at $u = 0$. As shown in Figure 8(d), the ratios δ_K/b and b_0/b increased and then decreased with x/L_h. The value of ratio δ_K/b was greater than 1.0 for $-1 < x/L_h < 0$, and less than 1.0 for $x/L_h < -1$. The value of ratio δ_K/b_0 ranged from 0.50 to 0.77, and the value of ratio b_K/b_0 ranged from 1.32 to 1.79. The results showed that in the return flow length range, the vertical position of the maximum TKE was higher than that of $0.5u_m$ and lower than that of $u = 0$. Half of the maximum TKE appeared above the zero velocity line. Since the value of b_0/b was in the range of 1.32–2.0 and the mixing region was in the range of $\delta < y < 2.0b$, the maximum TKE appeared in the mixing region.

CONCLUSIONS

The present study investigated the hydraulic characteristics of countercurrent jets (CCJs) on adverse-sloped beds, considering the effects of bed slopes and jet Froude numbers. The result showed that, compared to the horizontal bed, the adverse-sloped bed was mainly to reduce the length scale of CCJ, which could reduce the size and cost of the engineering design. The velocity distribution of CCJ with depth was divided into the boundary layer region, mixing region, and reverse surface jet region. The velocity distribution in the boundary layer region and the mixing region was similar to the classical wall jet. While in the reverse surface jet region, the velocity distribution of CCJ was significantly affected by the jet Froude number and bed slope. The jet Froude number and bed slope had no significant effect on the turbulence intensity and turbulence kinetic energy distribution (TKE) of CCJ. The maximum absolute turbulence intensity (ATI) along the water depth appeared at exactly half of the maximum velocity. The maximum TKE, on the other hand, appeared in the mixing region, above

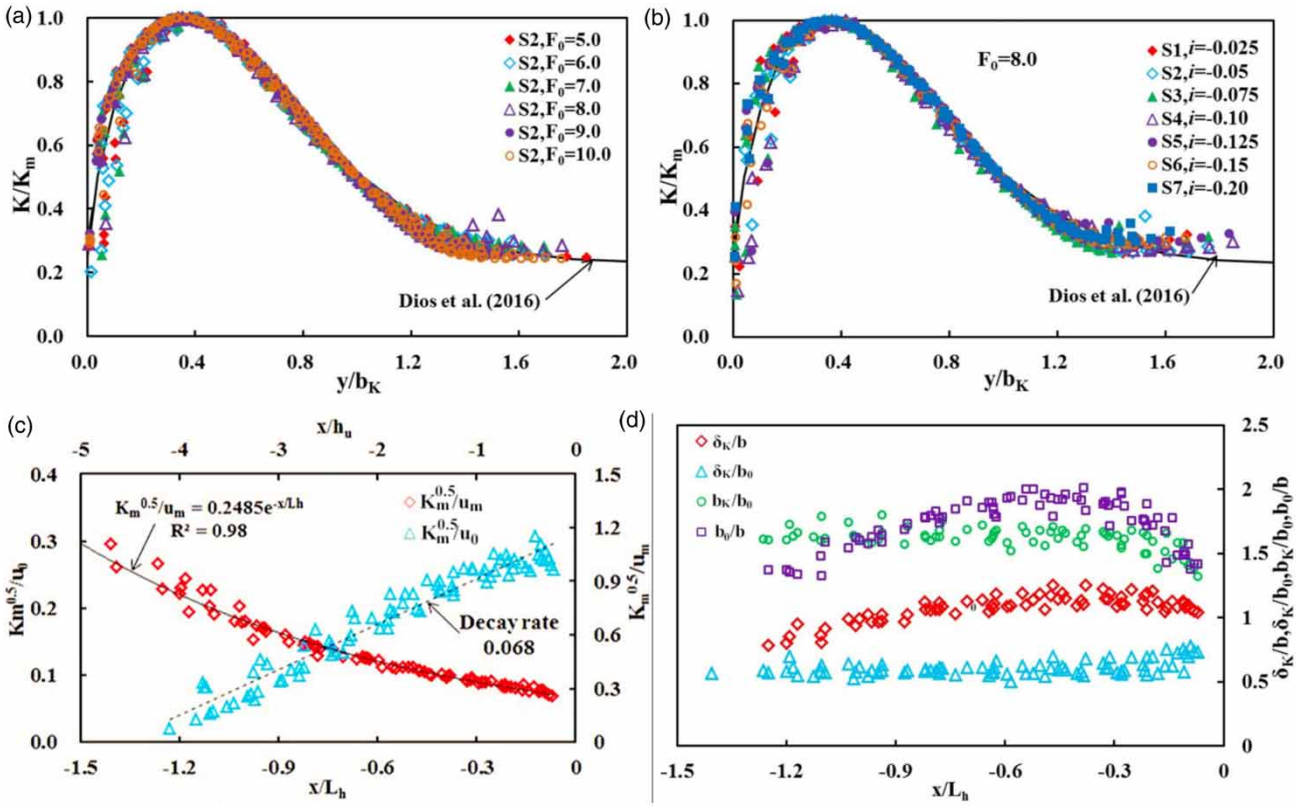

Figure 8 | (a-b) Variation of y/b_K against K/K_m; Variation of (c) Km0.5/u0; (d) δ_K/b, δ_K/b_0, b_K/b_0, against x/L_h.

where the maximum ATI appeared. The maximum relative turbulence intensity appeared at the junction of the mixing and the reverse surface jet region. Compared to the free jump on the adverse-sloped bed, the internal friction at the junction of the mixing region and reverse surface jet region caused an increase in the energy dissipation rate of CCJ. The bed slope did not affect the increase in the CCJ energy dissipation rate. In this study, the downstream of CCJ was free flow. If the downstream water depth is controlled, it can be used as an energy dissipation device for the outlet of a pressure spillway tunnel in hydraulic engineering. The results could provide a reference for the potential application of CCJ in the energy dissipation of hydraulic engineering.

DATA AVAILABILITY STATEMENT

All relevant data are included in the paper or its Supplementary Information.

REFERENCES

Bateni, S. M. & Yazdandoost, F. 2009 Hydraulics of B-F and F jumps in adverse-slope stilling basins. *Water Management* **162** (5), 321–327. doi:10.1680/wama.2009.162.5.321.

Beirami, M. K. & Chamani, M. R. 2010 Hydraulic jumps in sloping channels: length and energy loss. *Canadian Journal of Civil Engineering* **37** (4), 535–543. doi: 10.1139/L09-175.

Bejestan, M. S. & I Neisi, K. 2009 A new roughened bed hydraulic jump stilling basin. *Asian Journal of Applied Sciences* **2** (5), 436–445. doi: 10.3923/ajaps.2009.436.445.

Dey, S., Nath, T. K. & Bose, S. K. 2010 Fully rough submerged plane wall-jets. *Journal of Hydro-Environment Research* **4** (4), 301–316. doi: 10.1016/j.jher.2010.01.002.

Dios, M. D., Bombardelli, F. A., García, C. M., Liscia, S. O. & Parravicini, J. A. 2016 Experimental characterization of three-dimensional flow vortical structures in submerged hydraulic jumps. *Journal of Hydro-Environment Research* **15** (6), 1–12. doi:10.1016/j.jher.2016.11.001.

Ead, S. A. & Rajaratnam, N. 2002a Plane turbulent wall jets in shallow tailwater. *Journal of Engineering Mechanics* **128** (2), 143–155. doi: 10.1061/(ASCE)0733-9399(2002)128:2(143).

Ead, S. A. & Rajaratnam, N. 2002b Hydraulic jumps on corrugated beds. *Journal of Hydraulic Engineering-ASCE* **128** (7), 656–663. doi: 10.1061/(ASCE)0733-9429(2002)128:7(656).

Frizell, K. W. 2000 Effects of aeration on the performance of an ADV. In *2000 Joint Conference on Water Resources Engineering and Water Resources Planning and Management*, pp. 1–8. ASCE, Minneapolis. doi: 10.1061/40517(2000)299.

Ghaderi, A., Dasineh, M., Aristodemo, F. & Ghahramanzadeh, A. 2020 Characteristics of free and submerged hydraulic jumps over different macroroughnesses. *Journal of Hydroinformatics* **22** (6), 1554–1572. doi:10.2166/hydro.2020.298.

Hager, W. H. 1994 Countercurrent jet device. *Journal of Hydraulic Engineering-ASCE* **120** (4), 504–517. doi: 10.1061/(ASCE)0733-9429(1994)120:4(504).

Hager, W. H. & Bremen, R. 1989 Classical hydraulic jump; sequent depths. *Journal of Hydraulic Research* **27** (5), 565–585. doi: 10.1080/00221688909499111.

Islam, M. & Zhu, D. 2013 Kernel density–based algorithm for despiking ADV data. *Journal of Hydraulic Engineering-ASCE* **139** (7), 785–793. doi:10.1061/(ASCE)HY.1943-7900.0000734.

Josyula, E., Pinney, M. & Blake, W. B. 2015 Applications of a counterflow drag reduction technique in high-speed systems. *Journal of Spacecraft and Rockets* **39** (4), 605–614. doi: 10.2514/2.3850.

Lin, C., Hsieh, S. C., Lin, I. J., Chang, K. A. & Raikar, R. V. 2012 Flow property and self-similarity in steady hydraulic jumps. *Experiments in Fluids* **53** (5), 1591–1616. doi:10.1007/s00348-012-1377-2.

Liu, M., Zhu, D. Z. & Rajaratnam, N. 2002 Evaluation of ADV measurements in bubbly two-phase flows. In: *Hydraulic Measurements & Experimental Methods Specialty Conference*, pp. 1–10. doi: 10.1061/40655(2002)57.

Liu, M., Rajaratnam, N. & Zhu, D. Z. 2004 Turbulence structure of hydraulic jumps of low Froude numbers. *Journal of Hydraulic Engineering* **130** (6), 511–520. doi: 10.1061/(ASCE)0733-9429(2004)130:6(511).

McCorquodale, J. A. & Mohamed, M. S. 1994 Hydraulic jump on adverse slopes. *Journal of Hydraulic Research* **31** (1), 119–130. doi:10.1080/00221689409498793.

Pagliara, S. & Peruginelli, A. 2000 Limiting and sill-controlled adverse-slope hydraulic jump. *Journal of Hydraulic Engineering* **126** (11), 847–851. doi: 10.1061/(ASCE)0733-9429(2000)126:11(847).

Ramamurthy, A., Tudor, M., Han, S. S. & Vo, D. 2019 Characteristics of two-dimensional counter flowing wall jets. *Engineering and Computational Mechanics* **172** (4), 1–20. doi: 10.1680/jencm.18.00034.

Volchkov, E. P., Lebedev, V. P., Nizovtsev, M. I. & Terekhov, V. I. 1995 Heat transfer in a channel with a counter-current wall jet injection. *International Journal of Heat & Mass Transfer* **38** (14), 2677–2687. doi: 10.1016/0017-9310(94)00325-P.

Wang, L. & Diao, M. N. 2021 Velocity distribution characteristics of countercurrent jets. *Proceedings of the Institution of Civil Engineers – Water Management*, 1–11. https://doi.org/10.1680/jwama.20.00060.

Witt, A., Gulliver, J. S. & Shen, L. 2018 Numerical investigation of vorticity and bubble clustering in an air entraining hydraulic jump. *Computers & Fluids* **172** (7), 162–180. doi:10.1016/j.compfluid.2018.06.019.

Wu, S. & Rajaratnam, N. 1995 Free jumps, submerged jumps and wall jets. *Journal of Hydraulic Research* **33** (2), 177–212. doi: 10.1080/00221689509498670.

First received 26 April 2021; accepted in revised form 3 September 2021. Available online 15 September 2021